

Photodetachment Microscopy of hydrogen negative ion in a Uniform Magnetic Field

DE-HUA WANG*, SHENG LIU, SHAO-SHENG LI

School of Physics and Optoelectronic Engineering, Ludong University, Yantai 264025, China

The photodetachment microscopy of hydrogen negative ion in a uniform magnetic field is investigated on the basis of the semiclassical theory. Unlike the case of the photodetachment of hydrogen negative ion (H^-) in a uniform electric field, where only two trajectories of the detached electron arrived at a given detector and the photodetachment microscopy interference pattern is regular. For the photodetachment of H^- in a uniform magnetic field, due to the influence of the magnetic field force, more than two trajectories of the detached electron emitting from different directions may intersect at a given detector, thus creating a complex interference pattern in the electron flux distributions. Our calculation suggests that the electron flux distributions is not only related to the magnetic field strength, but also related to the electron energy and the position of the detector. Therefore, the interference pattern in the detached-electron flux distributions can be controlled by adjusting the magnetic field strength and the detached electron's energy. We hope that our studies may guide the future experimental researches in the photodetachment microscopy of negative ion in the magnetic field.

(Received December 5, 2012; accepted January 22, 2014)

Keywords: Photodetachment microscopy, Semiclassical theory, Electron flux, Magnetic field

1. Introduction

The photodetachment cross section of negative ions in presence of external electric or magnetic fields shows oscillations as a function of the photon energy[1-4]. Since the photo-detachment cross section is proportional to the integrated outgoing electron flux across a large enclosure in which the bound negative ions sits, therefore it is clear that the oscillation in the total cross section of negative ions in external fields reflects the oscillations in the electron flux distribution [5]. This predication was also observed experimentally by the photo-detachment microscopy. In early 1980s, Demo, Kondratovich and Ostrovsk first introduced the principle of photodetachment microscopy by studying the photodetachment process of negative ion in the presence of an electric field[6-8]. Microscopy is a kind of photoelectron imaging, by which we can directly observe the oscillatory structure of the wave function in a macroscopic scale [9-10]. Photodetachment microscopy opens a new way to measure electron affinities of neutral atoms by means of interference patterns with accuracy higher than any current *ab initio* calculations for multi-electron systems[11-14]. As a powerful technique to investigate electron dynamics, the microscopy has been used to study the photodetachment of negative ions in external electric and magnetic fields for many years both theoretically and experimentally. In the experimental aspect, Blondel *et al* first studied the photodetachment microscopy of Br^- in an electric field[15], they investigated a series of concentric interference fringes on the detector. Later, they performed the experiment for the photodetachment microscopy of O^- in an electric field[16]. Their experimental results were supported by the quantum calculation of Kramer *et al*[17].

In the theoretical aspect, Du had developed a semiclassical method to calculate the electron flux distributions in the photodetachment of H^- in an electric field[5]. He found that the interference of waves propagating along two distinctive paths from the region of the bound state of H^- to the same point induces oscillations in the electron flux distribution. His study can be considered as a primitive analysis for the photodetachment microscopy theoretically. Later, their semiclassical method has been extended to treat more complicated systems. In 2006-2007, Bracher, Delos and Gao *et al* studied the detached electron dynamics in external electric and magnetic fields [18-20]. Due to the influence of the electric and magnetic field forces, bifurcation effect appears in the detached electron trajectory and more than two trajectories can arrive at a given point on the detector, which lead to an intricate interference pattern in the electron flux distribution. Recently, with the development of the surface physics, the photodetachment of H^- near a metal surface has received a lot of attention [21-25]. Since the influence of the metal surface can be considered as an inhomogeneous electric field, Tang and Wang studied the photodetachment microscopy of H^- in an electric field or in a magnetic field near a metal surface[26-27]. In these early studies, they all discussed the photodetachment microscopy of H^- in an electric field or in the presence of electric and magnetic field. As to photodetachment microscopy of H^- in the presence of a purely magnetic field, the reports are relatively little. In 2010, Chaibi and coworkers studied the effect of an external static magnetic field on the electron interference ring patterns observed by the photodetachment microscope both experimentally and theoretically[28]. Their study shows: contrary to a previous study in weaker fields, where the overall

dimension of the interferogram was not modified, the effect of the magnetic field encompasses a regime of magnetic refocusing. Recently, Bracher and Gonzalez studied the electron dynamics in a uniform magnetic field [29]. Their study suggests that the features of the electron wave propagating from a point source in the presence of a purely magnetic field displays a richer variety of structure than in the cases of electric field or in parallel electric and magnetic fields. Inspired by their study, we study the photodetached electron flux distributions of hydrogen negative ion in the magnetic field with a semiclassical theory of photodetachment microscopy. We pay particular attention to the interference patterns in the flux distributions on the detector, and show how these patterns can be modified by the magnetic field strength and the electron's energy. Our studies may guide the future experiment research on the photodetachment microscopy of the negative ions in the presence of magnetic field. Atomic units are used throughout this work unless otherwise noted.

2. Theory and method

The schematic plot of the system is given in Fig. 1. Assuming the hydrogen negative ion sits at the origin with the detached electron loosely bound by a short-range, spherically symmetric potential. An external magnetic field B along the $+z$ axis is applied. A z -polarized laser is used for the photodetachment and a position sensitive detector is placed at $z = z_0 > 0$ plane.

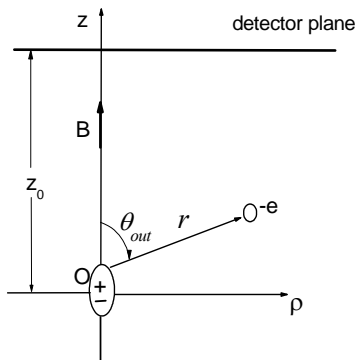


Fig. 1. The schematic plot of H^- in a uniform magnetic field. The magnetic field is along the $+z$ axis. H^- sits at the origin.

The physical picture of the photo-detachment process of H^- in the magnetic field can be described as follows: when the laser is on, the negative ion may absorb a photon of energy E_{ph} and the detached electron becomes an outgoing wave. The wave propagates away from the hydrogen atom in all directions, following classical trajectories. Guided by the classical electron trajectories,

the waves refract and fold over under the influence of the magnetic field [29]. In general, the electron can travel along more than one classical orbit from the hydrogen atom to the detector. As the electron moves far away from the ion, the wave functions can be constructed using the semiclassical approximation. Whenever two or more trajectories of the detached electron arrive at a given point on the detector, the corresponding waves interfere constructively or destructively, thus creating a complex interference pattern in the electron flux distributions on the detector. In order to calculate the electron flux distributions at a given point on the detector, we must find out all the trajectories of the detached electron that arrive at the given point in great detail.

The Hamiltonian for the detached electron in a uniform magnetic field has the following form (in cylindrical coordinates):

$$H = \frac{1}{2} \left(P_\rho^2 + \frac{L_z^2}{\rho^2} \right) + \frac{1}{2} P_z^2 + \omega_L L_z + \frac{1}{2} \omega_L^2 \rho^2 \quad (1)$$

in which $\omega_L = B/2c$ is the Larmor frequency, B is the magnetic field strength and c is the light speed.

Due to the cylindrical symmetry of the system, the z component of the angular momentum L_z is a constant of motion, which has been set to zero for the sake of convenient. Therefore, the Hamiltonian can be separated into the motion along the z -axis and the motion in the perpendicular x - y plane. By solving the Hamiltonian motion equations with the initial conditions $\rho=0$ and $z=0$, we get the classical motion equations of the detached electron at any time t [29]:

$$\begin{cases} \rho(t) = \frac{1}{\omega_L} k \sin \theta_{out} |\sin(\omega_L t)| \\ z(t) = kt \cos \theta_{out} \end{cases} \quad (2)$$

Where $k = \sqrt{2E}$ is the momentum of the detached electron, θ_{out} is the outgoing angle of the detached electron between the direction of the momentum and z -axis.

From the above equations, we find that the motion along the ρ direction is a cyclotron motion, with the cyclotron period $t_c = \pi / \omega_L$. The motion along the z direction is a simple uniform linear motion. Therefore, the trajectory of the detached electron in the magnetic field is a familiar helical orbit. Some classical trajectories of the detached-electron hitting the detector at a given point are shown in Fig. 2. From this figure, we find at a given point on the detector, several electron trajectories can pass through it.

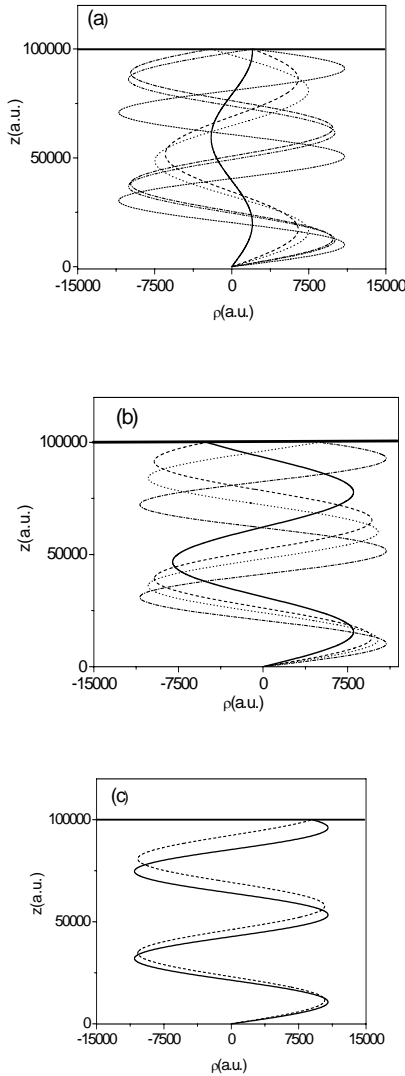


Fig. 2. Some classical trajectories of the detached electron reaching a given point on the detector plane. The detector is placed at $z=z_0=10^5$ a.u. plane, the magnetic field strength $B=1.0$ T and electron energy $E=0.01$ eV. (a): at the point $|\rho|=2000$ a.u., $z=10^5$ a.u.; (b): at the point $|\rho|=5000$ a.u., $z=10^5$ a.u.; (c): at the point $|\rho|=9000$ a.u., $z=10^5$ a.u.. Different trajectories are denoted by different lines.

Next, we find out all the trajectories of the detached electron that emitted from the origin and arrive at a given point on the detector plane. Supposing the detector is placed at $z=z_0$ plane above the z axis. From the motion equations of the detached electron (Eq.(2)), we can get the relation of the final position ρ at the detector plane versus the evolution time t :

$$\rho(t) = \frac{k}{\omega_L} |\sin(\omega_L t)| \sqrt{1 - \left(\frac{z_0}{kt}\right)^2} \quad (3)$$

Using the above formula, we plot a curve of the final position ρ at the detector versus time t , which is shown in Fig. 3, ρ_{ci} is the boundary point. We keep the electron's energy $E=0.01$ eV unchanged. The detector is placed at the plane localized at $z=z_0=10^5$ a.u. and the magnetic field strength B is decreased from 1.6 T to 0.1 T. Since the number of the trajectories that arrive at a given point on the detector is increased with the increase of the evolution time t . In our calculation, we limit the evolution time t within 5 cyclotron periods, i.e., the evolution time $t \leq 5\pi/\omega_L$. Next, we use the ρ - t diagram to find the trajectories arrived at a given point on the detector plane. We draw a line defined by $\rho=\text{constant}$ in this diagram and record the intersection points between this ρ - t curve and the $\rho=\text{constant}$ line. The number of intersection points gives the number of trajectories arriving at the same point ρ on the detector. For each intersection point, we can obtain the evolution time t that the electron arrived at the detector. By substituting t into Eq.(2), we can get the outgoing angle of the trajectory that can reach the detector:

$$\cos\theta_{out} = \frac{z_0}{kt}$$

Fig.3(a) shows the ρ - t curves with the magnetic field strength $B=1.6$ T. There is only one boundary point and the maximum impact radius ρ_{max} is relatively small. As the evolution time $t < 4\pi/\omega_L$, no detached electron trajectories can reach the detector. As $4\pi/\omega_L \leq t \leq 5\pi/\omega_L$, the whole region for ρ is divided into classically allowed region and classically forbidden region. For any points satisfy $0 < |\rho| < |\rho_{c1}|$, there are two values of the evolution time t corresponding to the same ρ , consequently there are also two detached electron's trajectories reaching the same position on the detector plane; for ρ larger than ρ_{c1} , there are no classical trajectories arriving at the detector plane. Fig. 3(b-f) shows the ρ - t curves with decreasing magnetic field strength. In Fig. 3(b), the magnetic field strength B is decreased to 1.2 T, the number of the boundary points is increased by one and the maximum impact radius ρ_{max} is increased. In the time domain, the whole region is divided into three separated intervals. As the evolution time $t < 3\pi/\omega_L$, no detached electron trajectories can reach the detector. As $3\pi/\omega_L \leq t \leq 5\pi/\omega_L$, the whole region for ρ on the detector plane is divided into two classically allowed region. For any points satisfy $0 < |\rho| < |\rho_{c1}|$, there are four values of the evolution time t corresponding to the same ρ , consequently there are four detached electron trajectories reaching the same position on the detector plane. For $|\rho_{c1}| < |\rho| < |\rho_{c2}|$, there are two

values of t corresponding to the same ρ , thus there are two detached electron trajectories reaching the same position on the detector; for ρ larger than $|\rho_{c_2}|$, no classical trajectories can reach the detector. As the magnetic field strength B is decreased from 1.6T to 0.1T, the number of the boundary point ρ_{ci} is increased, consequently the number of trajectories arriving at the same point ρ on the detector increases, which can be seen from the number of intersection points between a ρ - t curve and the ρ =constant line. Fig. 3(c) shows the ρ - t curve with magnetic field strength $B=1.0T$. The number of trajectories arriving at the same point on the detector is increased to six in the range of $0 < |\rho| < |\rho_{c_1}|$, some detached-electron trajectories are illustrated in Fig.2(a). For any point satisfying $|\rho_{c_1}| < |\rho| < |\rho_{c_2}|$, there are four detached-electron trajectories reaching the same point on the detector, as shown in Fig. 2(b). In the region $|\rho_{c_2}| < |\rho| < |\rho_{c_3}|$, only two trajectories interfere on the detector, as shown in Fig. 2(c). As we further

decrease the magnetic field strength, the number of the boundary points and detached electron trajectories reaching the same point on the detector continue to increase. In addition, the maximum impact radius ρ_{\max} becomes larger. In Fig. 3(e), the magnetic field strength B is decreased to 0.1T. The number of the boundary points is increased to 5. As $0 \leq t \leq 5\pi/\omega_L$, the whole range for the evolution time t is divided into five separated regions. In the classical allowed region $0 < |\rho| < |\rho_{c_1}|$, the number of the detached electron trajectories reaching the same point on the detector is increased to ten. As we further decreases the magnetic field, $0 < B < 0.1T$, the cyclotron period ($t_c = \pi/\omega_L$) of the electron becomes larger, thus the square term in Eq.(3) approximates to 1, then the value of the boundary point ρ_{ci} is nearly unchanged. Thus the number of the boundary point is invariant. In the region $0 \leq t \leq 5\pi/\omega_L$, the number of the boundary point is still 5. Therefore, in our study, we limit the magnetic field strength $B > 0.1T$.

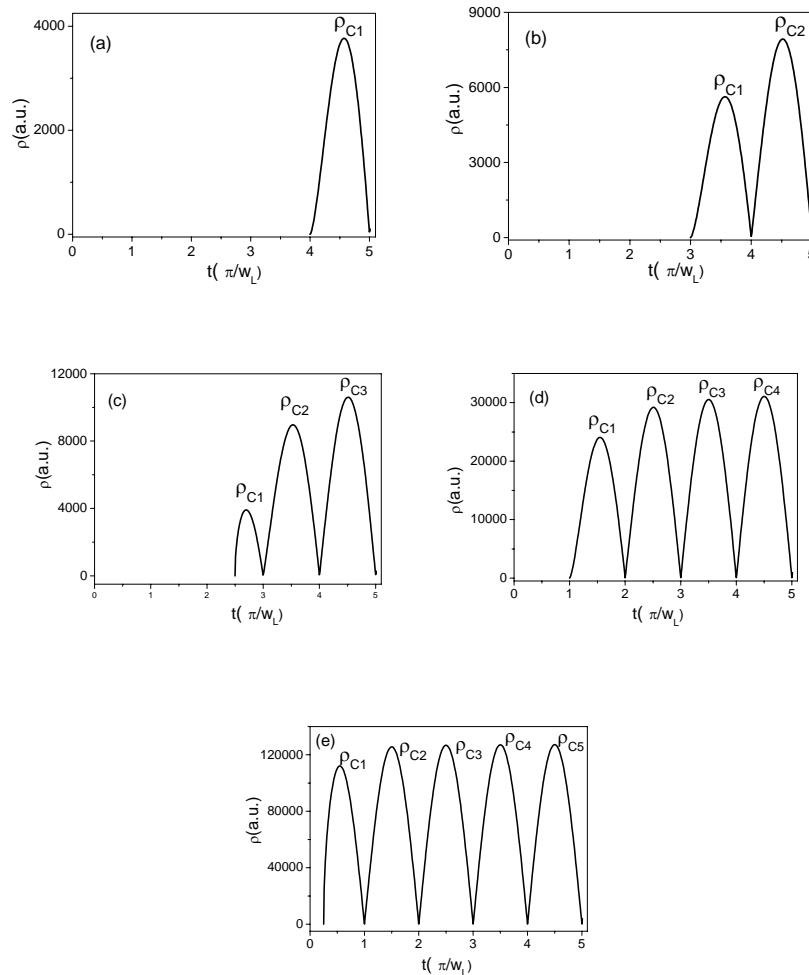


Fig. 3. Variation of the final position ρ as a function of the evolution time t of the detached electron in various magnetic field. Detached electron's energy $E=0.01\text{eV}$, and the detector is placed at $z_0=10^5\text{a.u.}$ plane. The magnetic fields are as follows: (a) $B=1.6T$, (b) $B=1.2T$, (c) $B=1.0T$, (d) $B=0.4T$, (e) $B=0.1T$.

3. Formula for electronic flux distributions of the detached-electron

Assuming the detector is put perpendicular to the z -axis at $z = z_0 > 0$ plane, the detached electron flux distributions on this detector can be calculated using the following formula [5, 26]:

$$\mathbf{j} = \frac{i}{2}(\psi_f \nabla \psi_f^* - \psi_f^* \nabla \psi_f) \quad (4)$$

Where ψ_f is the detached electron wave function in the magnetic field arriving at a given point on the detector. In order to calculate the wave functions of the electron, we divide the whole space into two spatial regions [26]: (1) The core region inside a small sphere with the radius $R \approx 5a_0$ (a_0 is the Bohr radius), where the atomic core field influence exists, while the magnetic field can be neglected; (2) The outer region, where the influence of the magnetic field is significant and the interaction between the detached electron and the hydrogen atom can be neglected. Therefore, we can use the semiclassical approximation to describe the electron's wave function[30-34]. The initial outgoing wave function on the spherical surface with the radius $R \approx 5.0a_0$ is given by[5]:

$$\psi_{out}(R, \theta, \varphi) = \frac{4B_0 k^2 i}{(k_b^2 + k^2)^2} \frac{e^{ikR}}{kR} \cos \theta_{out} \quad (5)$$

Where $k_b = \sqrt{2E_b}$, and E_b is the binding energy of the

$$J_j(t_j) = -\frac{k^3}{\omega_L} \sin(\omega_L t_j) \sin(\theta_{out}^j) [t_j \sin^2(\theta_{out}^j) \cos(\omega_L t_j) + \frac{1}{\omega_L} \sin(\omega_L t_j) \cos^2(\theta_{out}^j)] \quad (8)$$

Then the amplitude factor A_j is given by:

$$A_j = \frac{R}{k} \left| \frac{\omega_L}{\frac{t_j}{2} \sin^2(\theta_{out}^j) \sin(2\omega_L t_j) + \frac{1}{\omega_L} \sin^2(\omega_L t_j) \cos^2(\theta_{out}^j)} \right|^{1/2} \quad (9)$$

S_j is the classical action of the j -th trajectory:

$$S_j = \int p_\rho d\rho + \int p_z dz = k^2 \cos^2 \theta_{out}^j + k^2 \sin^2 \theta_{out}^j \left[\frac{1}{2} T_j - \frac{1}{4\omega_L} \sin(2\omega_L t_j) \right] \quad (10)$$

detached electron with the hydrogen atom. The normalization constant $B_0 = 0.31552$. As the outgoing wave propagates out from the sphere along one classical trajectory, its amplitude and phase vary. At a given point on the detector plane, the semiclassical wave function can be written in the form[26]:

$$\psi_f(r, \theta, \varphi) = \sum_{j=1}^n \psi_{out}(R, \theta, \varphi) A_j e^{i[S_j - \mu_j \pi / 2]} \quad (6)$$

Where the summation includes all the possible trajectories that begins at a point on the initial spherical surface and arrives at the final point on the detector. A_j is the amplitude, which measures the divergence of adjacent trajectories

from the j -th trajectory: $A_j = \left| \frac{J_j(t=0)}{J_j(t_j)} \right|^{1/2}$,

$J_j(t)$ is the Jacobian: $J_j(t) = \rho(t) \frac{\partial(z, \rho)}{\partial(t, \theta)}$. t_j is the evolution time of the j -th detached electron trajectory begins at a point on the initial spherical surface and arrives at the detector.

Substituting the classical motion equations of the detached electron (Eq.(2)) into the Jacobian, we can get the Jacobians at $t=0$ and t_j :

$$J_j(t=0) = kR^2 \sin(\theta_{out}^j) \quad (7)$$

μ_j is the Maslov index of the electron's trajectory, which can be calculated by counting the number of the singular points, including returning points, caustics and foci, etc[5].

Substituting the above equations into Eq.(6), we can get the semiclassical wave function at a given point on the

$$j_z(\rho, z) = \sum_i |\psi_i|^2 v_{iz} + \sum_{i < j} \text{Re}(\psi_i \psi_j^*) \cos(\chi_i - \chi_j) (v_{iz} + v_{jz}) \quad (11)$$

Where

$$\psi_i = \frac{4B_0 \cos \theta_{out}^i}{(k_b^2 + k^2)^2} \left| \frac{\omega_L}{\frac{t_i}{2} \sin^2(\theta_{out}^i) \sin(2\omega_L t_i) + \frac{1}{\omega_L} \sin^2(\omega_L t_i) \cos^2(\theta_{out}^i)} \right|^{1/2} \quad (12)$$

v_{iz} and v_{jz} are the z component of the electron velocities of trajectories i and j at a given point (ρ, z) respectively and the phase $\chi_i(r)$ is given by:

$$\chi_i(r) = S_i(r) - \frac{\mu_i \pi}{2}.$$

The first term in Eq.(11) is the classical electron flux distribution, and the second term represents the interference among different classical paths arriving at a given point on the detector.

4. Results and discussions

Using Eq. (11), we calculate the detached electron flux distributions of H^- in the magnetic field. Firstly, we fix the electron's energy ($E=0.01\text{eV}$), the position of the detector plane ($z_0=10^5\text{a.u.}$), and show how the flux distributions vary with the decrease of the magnetic field strength. We take the same magnetic field strength as given in Fig. 3. The results are shown in Fig. 4. From this figure, we find oscillatory structure appears in the electron flux distribution on the detector plane, which is caused by the interference effect between different trajectories arriving at the same point. Fig. 4(a) is the electron flux distribution with the magnetic field $B=1.6T$. Under this condition, only two detached-electron trajectories reaching the same position on the detector plane, therefore, the oscillatory structure in the electron flux distribution is regular and is similar to the photodetachment of H^- in an electric field [5].

detector plane. Using the expression for ψ_f in the flux formula in Eq.(4), we obtain the electron flux along the z -axis direction:

With the decrease of magnetic field strength, both the number of the detached-electron trajectories reaching the same position on the detector plane and the maximum impact radius ρ_{\max} are increased, as we can see from the ρ - t diagram. The oscillatory structure in the electron flux distribution becomes much more complex and the range of the flux distributions on the detector plane becomes larger. It is found that the flux distributions are divided into intervals by the boundary points ρ_{ci} as shown in Fig. 3. For example, Fig. 4(b) shows the electron flux distribution with the magnetic field $B=1.2T$. There are two boundary points $\rho_{c1} = 5743.33\text{a.u.}$ and $\rho_{c2} = 7992.27\text{a.u.}$. Correspondingly, the whole oscillating region is divided into two intervals. For $0 < |\rho| < |\rho_{c1}|$, there are four detached-electron trajectories reaching the same position on the detector plane, thus the oscillatory structure in the electron flux is much more oscillatory. For $|\rho_{c1}| < |\rho| < |\rho_{c2}|$, there are only two detached electron trajectories reaching the same position on the detector, and the oscillatory structure in the electron flux is relatively simple. As we further decrease the magnetic field strength, such as in Fig. 3(e), the magnetic field strength B is decreased to $0.1T$, the number of the boundary points is increased to five. Therefore the oscillatory structure in the electron flux distributions becomes much more complex and expands in a larger region.

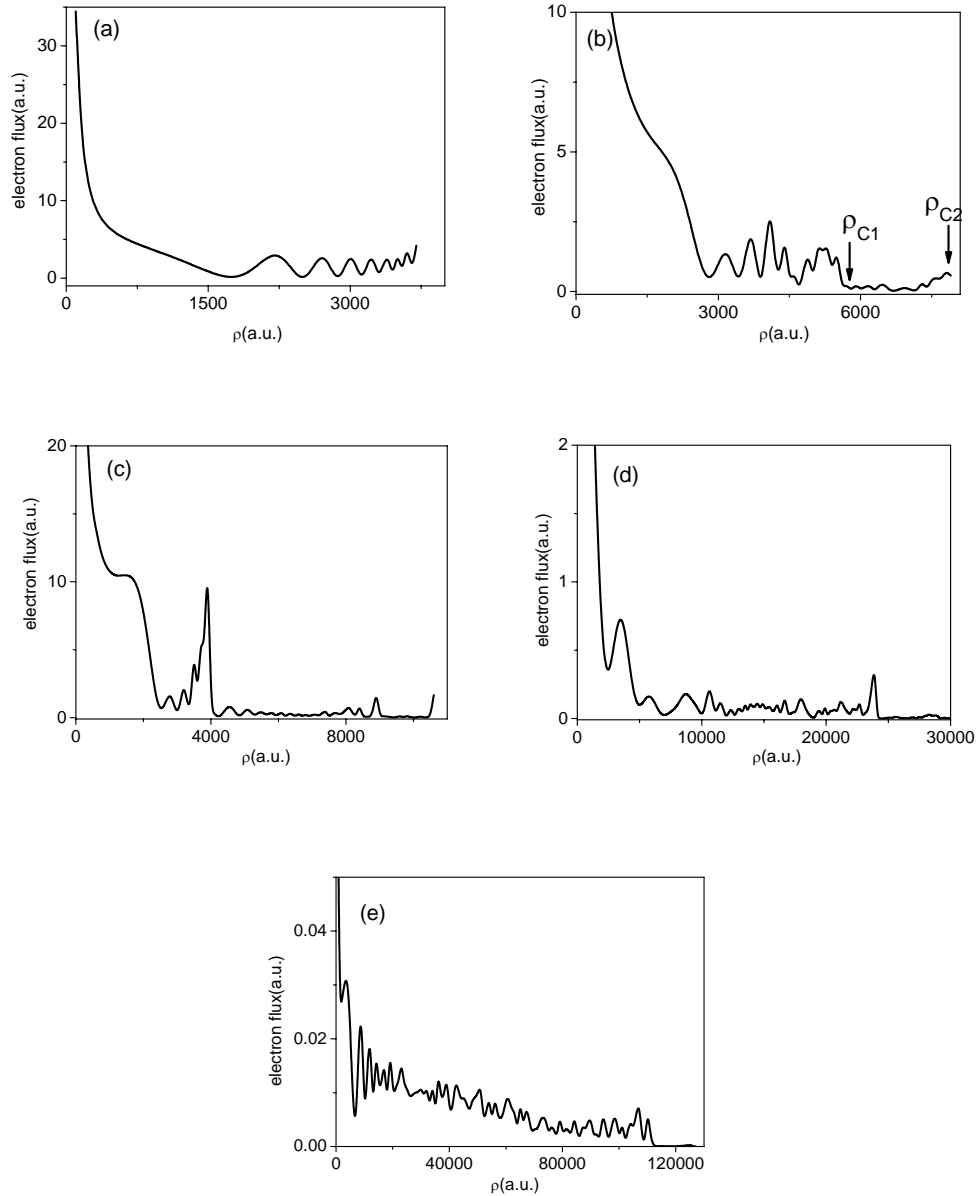


Fig. 4. Detached-electron flux distributions as a function of ρ at different magnetic field. Detached electron's energy $E=0.01\text{eV}$, and the detector is placed at $z_0=10^5\text{a.u.}$ plane. The magnetic fields are as follows: (a) $B=1.6\text{T}$, (b) $B=1.2\text{T}$, (c) $B=1.0\text{T}$, (d) $B=0.4\text{T}$, (e) $B=0.1\text{T}$.

Fig. 5 shows the variation of the detached electron flux distributions with the electron's energy. In our calculation, we fix the position of the detector plane at $z_0=10^5\text{a.u.}$ and keep the magnetic field strength $B=1.0\text{T}$ unchanged, then we increase the electron's energy. The corresponding ρ - t diagram for each case is given in the inset of each plot. Fig.5(a) is the flux distribution at a very

low energy $E=0.005\text{eV}$, the number of the detached-electron trajectories reaching the same position on the detector plane and the maximum impact radius ρ_{max} is small. So the oscillatory structure in the flux distributions is only limited in a small region and the oscillatory structure is not very complex in this case. With the increase of electron's energy, both the maximum

impact radius ρ_{\max} and the number of detached-electron trajectories reaching the same point on the detector increase. Thus the oscillation in the flux distributions

becomes much stronger with the increase of electron's energy. As we can see from Fig. 5(b-d).

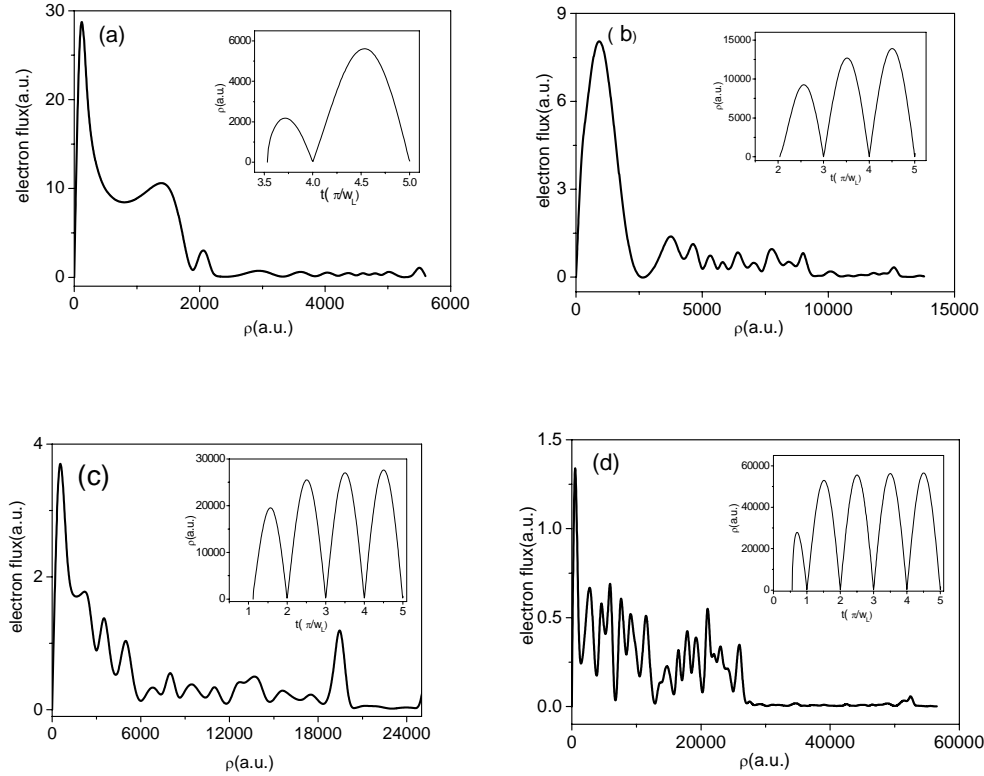


Fig. 5. The detached-electron flux distributions with the variation of the electron's energy. The detector is placed at $z_0=10^5$ a.u. plane, and the magnetic field strength B is 1.0T. The electron's energies are as follows: (a) $E=0.005$ eV, (b) $E=0.015$ eV, (c) $E=0.05$ eV, (d) $E=0.2$ eV. The corresponding $\rho-t$ curve is given as the inset in each plot.

In order to show the electron flux distributions on the detector surface clearly, we plot the 3-D contour image plot of the electron's flux distribution. The magnetic field strength $B=1.0$ T and the detached electron's energy $E=0.015$ eV. The contour image plot is shown in Fig. 6. It is found that the 3-D contour image plot of the detached electron flux distribution on the detector consists of a series of bright and dark rings, which are caused by the interference effect between different classical trajectories arrived on the detector. The bright rings correspond to the constructive interference and the dark rings correspond to destructive interference pattern on the detector. For example, at the central point on the detector, $\rho=0$, the electron flux at this point on the detector is the smallest, which corresponds to the destructive interference of the trajectories, correspondingly, there is a dark point at this point. Surrounding this point, the electron flux becomes increased, so there is a bright region in the 3-D contour image plot. This result is in excellent agreement with the results given in Fig. 5(b).

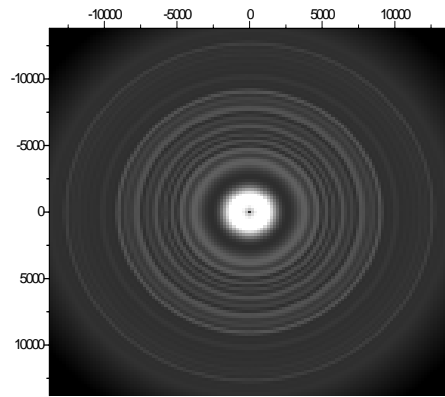


Fig. 6. 3-D contour image plot of the electron's flux distribution for H^- in a uniform magnetic field. The detector is placed at $z_0=10^5$ a.u. plane. The magnetic field strength $B=1.0$ T and the electron's energies $E=0.015$ eV.

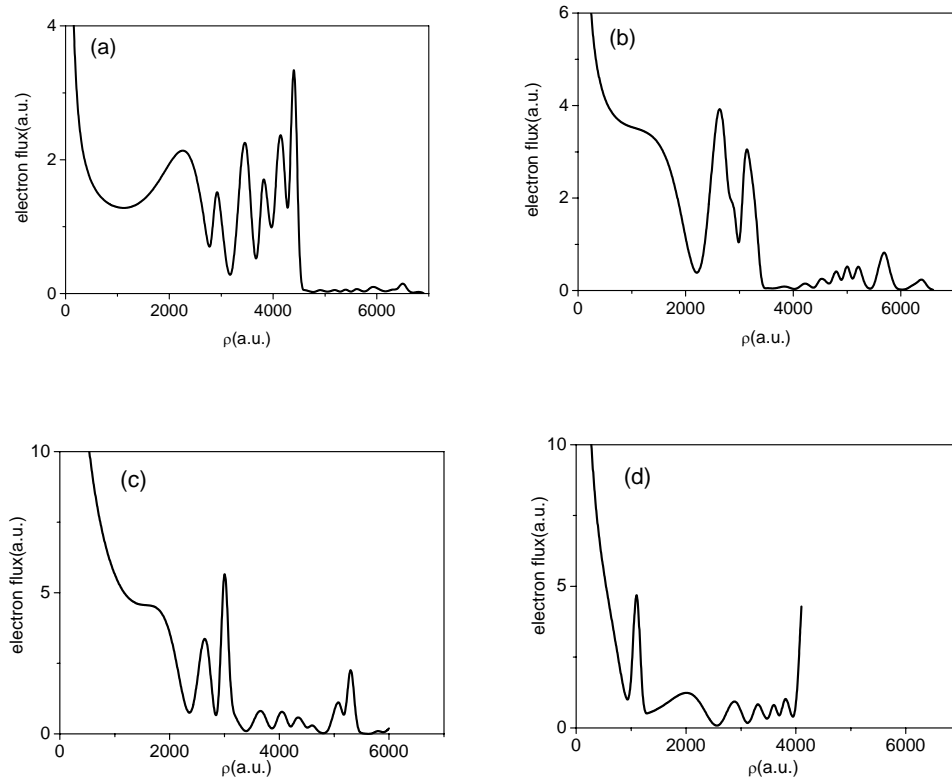


Fig. 7. The detached electron flux distributions with the variation of the detector plane. The electron's energy $E=0.003\text{eV}$, and the magnetic field strength $B=1.0T$. The position of the detector plane is as follows: (a) $z_0=10^4\text{a.u.}$, (b) $z_0=3\times 10^4\text{a.u.}$, (c) $z_0=5\times 10^4\text{a.u.}$, (d) $z_0=8\times 10^4\text{a.u.}$.

Finally, we study the variation of the detached electron flux distributions with the position of the detector plane. In our calculation, we keep the electron's energy $E=0.003\text{eV}$ and the magnetic field strength $B=1.0T$ unchanged. Then we change the position of the detector plane. The results are given in Fig.7. From this figure, we find the oscillatory structure and the oscillating region in the detached-electron flux distributions varies with the position of the detector plane. If the distance from the ion to the detector plane is relatively small, for example, in Fig.7(a), $z_0=10^4\text{a.u.}$, the number of the detached-electron trajectories reaching the same point on the detector is large, therefore the oscillatory structure in the electron flux distributions becomes much more complex. As we move the detector plane far away from the ion, the number of the detached-electron trajectories reaching the same point on the detector becomes decreased, so the oscillatory structure in the electron flux distributions becomes relatively simple. As we can see from Fig.7(b-d) clearly.

5. Conclusion

We study the photodetachment microscopy of H^- in a magnetic field using the semiclassical theory. The semiclassical wave function for the detached electron has been obtained and the electron flux distributions at a given point on the detector are calculated. The results show that the electron flux distributions on the detector plane are related to the magnetic field strength, the electron energy and the distance from the ion to the detector plane sensitively. With the decrease of the magnetic field strength, the number of the electron's trajectories reaching the detector becomes increased. Therefore, the oscillatory structures in the flux distributions become much stronger. In addition, we find that the oscillation in the flux distributions becomes strengthened with the increase of the detached electron's energy. Presently no experiments on the photodetachment microscopy of H^- in a magnetic field have been carried out. We hope that our results will guide future experiment research on the photodetachment microscopy of the negative ions in the presence of magnetic field.

Acknowledgements

This work is supported by the National Natural Science Foundation of China (Grant Nos. 11374133, 11074104, 10604045), and a Project of Shandong Province Higher Educational Science and Technology Program of China(Grant No. J13LJ04).

References

- [1] H. C. Bryant, Phys. Rev. Lett. **58**, 2412 (1987).
- [2] N. D. Gibson, B. J. Davies, D. J. Larson, Phys. Rev. A **47**, 1946 (1993).
- [3] N. D. Gibson, M. D. Gasda, K. A. Moore, D. A. Zawistowski, C. W. Walter, Phys. Rev. A **64**, 061403 (R) (2001).
- [4] M. L. Du, J. B. Delos, Phys. Rev. A **38**, 5609(1988).
- [5] M. L. Du, Phys. Rev. A **40**, 4983(1989).
- [6] Y. Demo, V. Kondratovich, V. Ostrovskii, JETP Lett. **34**, 403 (1982).
- [7] V. D. Kondratovich, V. N. Ostrovsky, J. Phys. B **17**, 1981 (1984).
- [8] V. D. Kondratovich, V. N. Ostrovsky, J. Phys. B **17**, 2011 (1984).
- [9] Ch. Bordas, F. Lépine, C. Nicole, M. J. J. Vrakking, Phys. Rev. A **68**, 012709 (2003).
- [10] H. F. Yang, L. Wang, X. J. Liu, H. P. Liu, Chin. Phys. B **20**, 063203 (2011).
- [11] C. Valli, C. Blondel, C. Delsart, Phys. Rev. A **59**, 3809 (1999).
- [12] C. Blondel, C. Delsart, F. Goldfarb, J. Phys. B **34**, L281 (2001).
- [13] C. Blondel, W. Chaibi, C. Delsart, C. Drag, Eur. Phys. J. D **33**, 335 (2005).
- [14] T. Anderson, Phys. Rep. **394**, 157 (2004).
- [15] C. Blondel, C. Delsart, F. Dulieu, Phys. Rev. Lett. **77**, 3755 (1996).
- [16] C. Blondel, C. Delsart, F. Dulieu, C. Valli, Eur. Phys. J. D **5**, 207 (1999).
- [17] T. Kramer, C. Bracher, M. J. Kleber, Phys. A **35**, 836 1(2002).
- [18] C. Bracher, T. Kramer, J. B. Delos, Phys. Rev. A **73**, 062114 (2006).
- [19] C. Bracher, J. B. Delos, Phys. Rev. Lett. **96**, 100404 (2006).
- [20] S. Gao, G. C. Yang, S. L. Lin, M. L. Du, Eur. Phys. J. D **42**, 189 (2007).
- [21] H. J. Zhao, M. L. Du, Phys. Rev. A **79**, 023408 (2009).
- [22] K. K. Rui, G. C. Yang, Surf. Sci. **603**, 632 (2009).
- [23] B. C. Yang, M. L. Du, J. Phys. B: At. Mol. Opt. Phys. **43**, 035002 (2010).
- [24] K. Y. Huang, D. H. Wang, J. Phys. Chem. C. **114**, 8958 (2010).
- [25] D. H. Wang, J. Elect. Spect. **177**, 30 (2010).
- [26] T. T. Tang, D. H. Wang, J. Phys. Chem. C, **115**, 20529 (2010).
- [27] T. T. Tang, D. H. Wang, S. S. Wang, Chin. Phys. B **21**, 073202 (2012).
- [28] W. Chaibi, R. J. Peláez, C. Blondel, C. Drag, C. Delsart, Eur. Phys. J. D **58**, 29 (2010).
- [29] C. Bracher, A. Gonzalez, Phys. Rev. A **86**, 022715 (2012).
- [30] L. B. Zhao, J. B. Delos, Phys. Rev. A **81**, 053417 (2010).
- [31] L. Wang, H. F. Yang, X. J. Liu, H. P. Liu, M. S. Zhan, J. B. Delos, Phys. Rev. A **82**, 022514 (2010).
- [32] H. J. Zhao, M. L. Du, Phys. Rev. E **84**, 016217 (2011).
- [33] D. H. Wang, S. S. Li, Y. H. Wang, H. F. Mu, J. Phys. Soc. Jpn. **81**, 114301 (2012).
- [34] D. H. Wang, X. M. Tan, G. Zhao, J. Phys. Soc. Jpn. **82**, 164301 (2013).

*Corresponding author: lduwdh@163.com